IEEE Access
Multidisciplinary | Rapid Review | Open Access Journal

Received 16 August 2024, accepted 2 September 2024, date of publication 10 September 2024,
date of current version 19 September 2024.

Digital Object Identifier 10.1109/ACCESS.2024.3456833

RESEARCH ARTICLE

Electromagnetic Characteristics Interpretation of Partial Discharge Phenomena at Variable Distance in High-Voltage Systems

S. M. KAYSER AZAM[1], JUN QIANG CHAN[1], MOHAMADARIFF OTHMAN[1], WONG JEE KEEN RAYMOND[1], (Senior Member, IEEE), HAZLEE AZIL ILLIAS[1], (Senior Member, IEEE), TARIK ABDUL LATEF[1], A. K. M. ZAKIR HOSSAIN[2], (Member, IEEE), HAMASKUTTY VETTIKALLADI[3], ALI M. ALMUHLAFI[3], (Senior Member, IEEE), MOHAMED HIMDI[4], AND ABD KARIM ABD RAHMAN[5]

[1]Department of Electrical Engineering, Universiti Malaya, Kuala Lumpur 50603, Malaysia
[2]Centre for Telecommunication Research and Innovation, Fakulti Teknologi Kejuruteraan dan Elektrik dan Elektronik, Universiti Teknikal Malaysia Melaka, Durian Tunggal, Melaka 76100, Malaysia
[3]Electrical Engineering Department, College of Engineering, King Saud University, Riyadh 11421, Saudi Arabia
[4]Institut d'Electronique et des Technologies du numeRique (IETR), University of Rennes 1, 35042 Rennes, France
[5]Project Delivery and Technology Division, Petroliam Nasional Berhad (Petronas), Kemaman, Terengganu 243000, Malaysia

Corresponding author: Mohamadariff Othman (mohamadariff@um.edu.my)

This work was supported in part by Universiti Malaya, Malaysia through the RU Geran-Fakulti Program under Grant GPF008A-2023; in part by the Researchers Supporting Project, King Saud University, Riyadh, Saudi Arabia, under Grant RSP2024R482; and in part by the Ministry of Higher Education Malaysia through Malaysia International Scholarship, in 2022, and Fundamental Research Grant Scheme under Grant FRGS/1/2022/TK07/UM/02/57.

ABSTRACT Insulations at high voltage (HV), whether in HVAC or HVDC systems, often encounter an unwanted partial discharge (PD) phenomenon. PD poses a potential danger to HV insulation and can eventually lead to equipment failures. Out of all electromagnetic (EM) sensing techniques for PD diagnosis, the ultra-high frequency (UHF) method has gained popularity as it allows non-invasive detection at varying distances from PD defects. The EM behavior of PD is significantly affected by the distance between a PD defect and a UHF sensor. This effect varies for different PD defects under different HV conditions. So, considering variable distances, there is a need to analyze EM characteristics of different PD phenomena at different HV conditions. To the best of our knowledge, for the first time, electromagnetic characteristics of different PD defects are experimentally investigated in this work by capturing PD signals from variable distances in both HVAC and HVDC conditions and individually validating their characteristics with EM radiation theories. For wirelessly capturing PD signals, a new UHF sensor is designed with a modified elliptical-shaped antenna on an FR-4 material. The fabricated sensor provides an average realized gain of about 3.66 dBi while covering more than 97% of the total UHF range for PD detection. Applying HVAC, HVDC+, and HVDC–, PDs from three defects (surface, void, free wire) are captured from 1–4 m distances. Interpreted results show that EM radiation in the UHF range from a PD defect is heavily impacted by its detection distance and defect formation despite applied voltage and other conditions being unchanged for the defect. This investigation is particularly beneficial to the variable distance-based PD diagnosis, such as PD localization and handheld PD detection at HVAC/HVDC open substations.

INDEX TERMS Partial discharge, electromagnetic characteristics, UHF antenna, PD detection distance, HVAC/HVDC, open substations.

The associate editor coordinating the review of this manuscript and approving it for publication was Pavlos I. Lazaridis.

I. INTRODUCTION

Radiation characteristics of electromagnetic (EM) transmitters, being deliberately designed for wireless communications,

are well-formulated and predictable for practical cases. However, EM radiations from unexpected and random phenomena are difficult to predict [1], [2], [3]. Partial discharge (PD) is such a phenomenon in high voltage (HV) insulations. PD, being a random and unwanted event caused by insulation defects in HV conditions, radiates EM waves as an outcome of its occurrence. When PD occurs, it appears in many forms such as electric current impulse, acoustic signals, chemical decomposition, EM signals in ultra-high frequency (UHF) range etc. [4], [5] which have their own sensing methods. Since PD is a potential threat in HV which eventually damages equipment, PD signals can be diagnosed by using any of those sensing methods. Conventionally, coupling capacitor-based method is used to sense the electric impulses during PD occurrence which is followed by the IEC 60270 standard. Although some of the recently available coupling capacitors can perform online PD diagnosis, however, this method is still invasive since coupling capacitor needs a direct contact with the PD-affected equipment for sensing purposes [6]. So, UHF method is drawing more attention nowadays because it is a non-invasive and contactless method of online PD diagnosis even at distances from defects. Currently, the IEC TS 62478:2016 is used as the standard for PD diagnostics by UHF method [7].

In the UHF method, the key component is the UHF sensor. Generally, antennas are used as sensors in PD detection (PDD) systems since they are electrically small in the UHF range [4]. Different types of UHF antennas are applied as UHF sensors for PDD such as Archimedean spiral antenna (ASA) [8], planar monopole antenna (PMA) [9], [10], [11], coplanar waveguide (CPW) antenna [12], and so on. In this regard, PMAs are becoming more popular because their low-profile, wideband, and omnidirectional radiation characteristics enable them to detect PD from any isotropic directions over wide range of frequencies while occupying small spaces in the PDD system [13]. It is important to remember that UHF antennas, while working as PD sensors, operate only in the signal receiving mode. Hence, amplitudes of different PD signals detected by the same UHF antenna-sensor are not same since EM characteristics of PD signals depend on the PD defect type and the HV condition applied to the dielectric insulation [14], [15]. On the other hand, amplitudes of detected PD signals also depend on the distance between a PD defect and the UHF antenna-sensor in the far-field radiation zone. Thus, electromagnetic characterization of different types of PD defects in HVAC and HVDC should be performed, especially for variable distance-based PD diagnosis in open substations. It is because the distance between PD defects and UHF sensors varies during PD localization and PD detection by handheld operations in open substations. Previously, EM wave characteristics of PD have been discussed in some works but mostly for gas insulated switchgear (GIS) [16], [17], [18] or power transformer [19], [20], [21], [22] where the equipment's metallic enclosure has strong influences on EM behaviors of PD. Also, UHF sensors are typically fixed at positions inside GISs and power transformers. Whereas in open substations, UHF sensor positions vary during handheld operations for PD detection and localization. EM behaviors of different PD defects can be understood better in open substations as far-field EM radiation is not blocked by metallic enclosures. Despite some higher frequency components from telecommunication sources can act as EM noises in open substation, onsite metallic cage and filtering methods are utilized [13] to minimize the external noises. Therefore, in line with theoretical concepts and formulations [23], [24], [25], EM characteristics of PD defects need to be particularly investigated for open substations both in HVAC and HVDC conditions because in real applications PD defects must be analyzed in whatever the situation is.

In this work, a comprehensive investigation is conducted into EM characteristics of three particular PD defects, namely free wire (open-ended electrode configuration), surface (electrode-insulation-electrode configuration), and void (air gap inside insulation configuration) defects, in open substations. Under HVAC, HVDC+, and HVDC– settings, these characteristics are measured over variable distances. To facilitate the EM characterization, a new UHF antenna sensor is developed. This work provides practical insights into the EM radiation by PD defects, to improve the performance of PD detection and localization. The article is structured as follows: Section II gives an overview of the procedure, Section III presents the theoretical background of EM radiation from PD, Section IV details the development of the UHF sensor, Section V describes the experimental setup and provides information on the PD defects studied, Section VI presents the experimental results and provides analyzed interpretations of the EM characteristics of these PD defects in HVAC, HVDC+, and HVDC– settings, and Section VII concludes the article.

II. OVERVIEW OF INTERPRETATION PROCEDURE

Fig. 1 overviews the characteristics interpretation procedure of this work. It is important to understand influences of some factors in measuring electromagnetic (EM) characteristics of a PD defect in UHF method which are presented in Fig. 1(a). Typically, EM characteristics of PD defects are understood by analyzing peak-to-peak voltage (V_{PP}) detected by UHF antenna-sensors. In this regard, defect type, defect dimensions, applied high-voltage level (V_{HV}), UHF antenna-sensor properties, sensing distance, sensing medium, ambient conditions etc. are some of the most influential factors.

Generally, PD characteristics interpretation is performed by analyzing the characteristics of a PD defect at a fixed distance in terms of the defect's dimensional variation. This does not fully reveal the far-field radiation characteristics of a PD defect. In this research, factors illustrated in Fig. 1(a) are considered in a way so that PD characteristics interpretation focuses on far-field electromagnetic radiation behaviors of specific PD defects in terms of variation in the sensing distance. Here, three particular types of PD defects with fixed dimensions are chosen, namely surface, free-wire, and void.

Since commercially available UHF sensors are expensive and mostly have low gain, a new planar monopole antenna (PMA) is prepared as the UHF sensor for this research. The PMA is developed with desired properties on a low-cost FR-4 substrate. During characterization, although some low-power telecommunication signals are available in the higher frequency regions, most of the lower frequency signals from radio and television sources are blocked by the shielding cage in the testbench. Ambient conditions along with sensing medium are kept unchanged throughout the characterization. In turn, out of all the factors illustrated in Fig. 1(a), applied high-voltage (V_{HV}) level and sensing distance (D) remain variable for the characterization of a particular PD defect.

PD being a stochastic process, its randomness in electromagnetic characteristics depends on several factors, such as applied voltage, defect type, defect dimensions, UHF sensor properties, sensing medium, ambient conditions, and sensing distance, as illustrated in Fig. 1(a). When all these parameters remain constant for a specific sensing distance, the detected voltage amplitudes are consistent across different PD events from that distance. Although there are variations in peak-to-peak amplitudes, they generally maintain an average level. Typically, in this case, detected voltage amplitudes are more consistent than their corresponding electromagnetic frequencies. In this research, to ensure accuracy, the raw data for each applied voltage were collected three times, and the average value was used. So, when a voltage is applied to a PD defect, the oscilloscope's data collection amplitude level is set by observing the corresponding maximum detected voltage first. Once this level is determined, three consecutive peak-to-peak data sets are collected under the same applied voltage condition. This process is repeated for each applied voltage condition at a specific sensing distance. The same procedure is then followed for other sensing distances. By adhering to this method, we characterize the effect of sensing distance on PD detection, despite the inherent randomness of PD events.

Fig. 1(b) demonstrates how a single plotted data is extracted for a PD defect that is located at a particular distance i.e., sensing distance (D). For each V_{HV}, the corresponding V_{PP} is detected, and detection begins with the PD inception voltage (PDIV) until the breakdown voltage (BDV) of a PD defect. After detecting all V_{PP} for corresponding all V_{HV}, a V_{PP} versus V_{HV} plot is made to analyze EM characteristics of the PD defect at distance ''D''. This procedure continues with the variation of ''D'' for a PD defect. Once enough data are extracted with the variation of ''D'' for a particular PD defect, then the same procedure is applied to another PD defect to analyze its EM characteristics. For EM characteristics analysis, EM radiation models of PD defects are utilized.

III. ELECTROMAGNETIC RADIATION MODELS OF PARTIAL DISCHARGES

Partial discharge (PD) defects release the EM radiation in the UHF range. Since free wire, surface and void are considered as PD defects in this paper, it is important to understand the EM characteristics of these defects based on the EM radiation

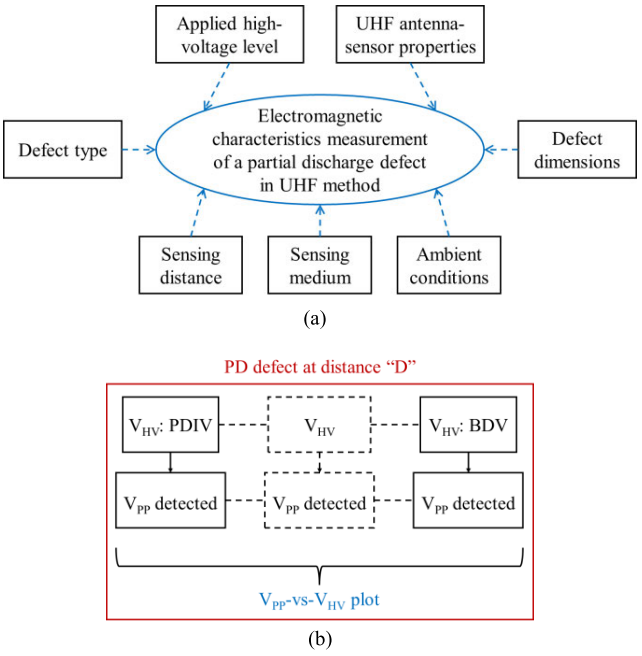

FIGURE 1. Overview: (a) factors influencing EM characteristics of PD defect in UHF method (b) single plotted data extraction at a particular distance.

models of PD in terms of point charge [24] and dipole [26] as shown in Fig. 2.

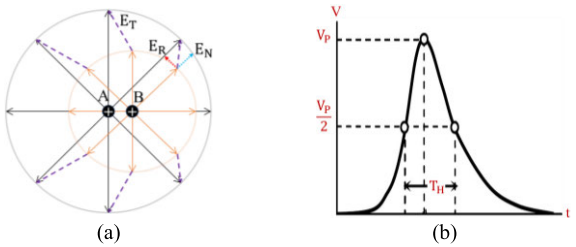

FIGURE 2. EM radiation of partial discharge: (a) charge acceleration (b) voltage waveform.

A. EM RADIATION FROM POINT CHARGE

Static charges, yet providing electric field, cannot exhibit EM radiation because magnetic field requires a current flow by the movement of charges. Again, EM radiation is not found in the circular direction from a charge when the charge has movement but with no acceleration or deceleration. So, EM radiation from a charge is found with omnidirectional pattern only when the charge accelerates or decelerates by decaying EM energy. This is because an accelerating or deaccelerating point charge has the radiating behavior of a monopole antenna which typically radiates EM waves in all isotropic directions. Hence, an observer from any of these positions experiences directional radiation even though the point charge actually radiates with an omnidirectional pattern. As in Fig. 2(a), for a charge movement with acceleration (from position A to B), the E_R component of the electric field bent at an angle emits radiation. Here, the total electric field

(E_T) is a resultant of E_R because there is no electric field component (E_N) along the charge movement due to the absence of a travelling wave. If there is a constant movement of the charge after position B, then EM radiation is found by electric (E_T) and magnetic (H_T) fields as [24].

$$E_T = \frac{aQ\sin\theta}{4\pi lc^2\varepsilon_0}, \tag{1}$$

$$H_T = \frac{aQ\sin\theta}{4\pi lc}. \tag{2}$$

Here, a is the charge acceleration, Q is the value of the point charge, θ is the angular value of between charge acceleration and observation position, l is the travelling distance of the charge within a period (T), c is the light speed, and ε_0 is the dielectric permittivity of the air. The EM radiation from E_T and H_T in turn has a omnidirectional pattern that resembles a donut shape [23], [24]. Hence, the radiated EM energy from a point charge of a PD defect is distributed to the far-field region in all isotropic directions. Thus, such an EM radiation can be detected by placing a UHF sensor at distances. A total EM energy can be obtained over the entire isotropic directions by integrating the following Poynting vector (S),

$$S = E_T \times H_T = c\varepsilon_0 E_T^2 = \frac{a^2Q^2\sin\theta}{16\pi^2 l^2 c^3\varepsilon_0}. \tag{3}$$

Now, from the Larmor's Formula, total radiated EM power can be obtained as [24],

$$P_R = \frac{a^2Q^2}{6\pi\varepsilon_0 c^3}. \tag{4}$$

Notice that distribution of P_R varies from one PD defect to another based on its accelerated charges in an HV condition. However, P_R typically decreases over time for increasing the distance between PD defect and UHF sensor.

B. EM RADIATION FROM DIPOLE

For defects such as voids, surface, and laminations inside HV insulations, where dielectric mediums exist beside the air, electric dipole moments are generated when charges (Q) with opposite polarities are spaced by a gap (d). In Fig. 2(b), voltage waveform of V(t) is observed when EM wave is radiated from a PD defect. In V(t), VP is the peak voltage and TH is the half-amplitude time. This is expressed as [26],

$$V(t) = \frac{\Delta V}{2} erf\left[\frac{t}{\left(\frac{T_H}{2\sqrt{\log 2}}\right)}\right] = \frac{Q}{2C_g} erf\left[\frac{t}{t_0}\right] \tag{5}$$

In this expression, ΔV is the voltage variation during the time t, erf is the error function, and C_g is the gap capacitance. From the Hertz vector, the electric field (E_D) of the dipole in the far-field EM radiation is expressed as [24] and [26],

$$E_D = \frac{Q.d}{2\varepsilon_0\varepsilon_r c^2\sqrt{2e_C}\pi^{1.5}t_0^2 D_O}\sqrt{2e_c}\left(\frac{t-\frac{y}{c}}{t_P}\right)e^{-\left(\frac{t-\frac{y}{c}}{t_0}\right)^2}. \tag{6}$$

Here, ε_r is dielectric constant of HV insulating material, e_c is electron charge, D_O is distance between origin and dipole, and y is axial length on the EM wave propagation direction. This implies that EM radiation of PD works only in one coordinate. It is clear that EM radiation intensity is inversely proportional to HV insulation's dielectric constant and duration of a PD impulse. This further impacts on the voltage level of PD signals detected by UHF sensor when the distance between PD defect and UHF sensor is variable. UHF sensor with the right specifications is also essential.

IV. UHF SENSOR FOR PD PHENOMENA DETECTION

A. SENSOR DESIGN AND SIMULATION

In PD applications, the average realized gain of a passive UHF sensor should be more than 2 dBi. This is difficult to achieve because UHF sensors are typically based on planar antennas that exhibit poor gain performance on commercially available substrates. So, commercially available UHF sensors mostly use amplification circuits to solve this issue which makes them expensive. [4], [13]. An alternative is to manually develop passive UHF sensor so that its design technique improves the average realized gain without using active components for amplification. Also, this offers freedom in specifying sensor's desired performance according to a particular condition. Thus, for this work, a new sensor is developed on a low-cost FR-4 substrate. In this regard, Archimedean spiral antennas (ASAs) offer high gain which makes them successful in PD detection applications, however typically, their unidirectional radiation pattern limits the ability to capture PD signals from any isotropic radial direction. So, a planar monopole antenna (PMA) is selected to design our UHF sensor since PMAs have omnidirectional radiation pattern with wideband characteristics and sufficient realized gain. Still, the average realized gain should be increased more to improve the PD detection ability of our UHF sensor. The UHF sensor is developed as in Fig. 3(a) by designing a PMA as modified elliptic-shaped antenna (MESA) with a slot on the ground layer. MESA is designed on a FR-4 substrate with a length (L) of 20 cm and a width (W) of 16 cm while the feedline has a width of w_f as [13],

$$w_f = \frac{7.48\times h}{e^{(Z_0\frac{\sqrt{\varepsilon_D+1.41}}{87})}} - 1.25\times t. \tag{7}$$

Here, $h = 1.6$ mm is substrate height, Z_0 is characteristics impedance matched by the standard normalized impedance of 50 Ω, $\varepsilon_D = 4.2$ is dielectric constant of FR-4, and $t = 0.035$ mm is the trace-thickness of the conductive layer while the feedline length (L_f) is 115.4 mm. For design and simulation, CST Studio Suite 2023 is utilized by adopting finite element method (FEM) and time-domain hexahedral transmission line method solver with −40 dB accuracy on 15 cells per wavelength within a boundary of 0.1−10 GHz frequency range. The radiating layer, joining the feedline as in Fig. 3(a), is designed by elliptical patch (E_P) and rectangular patch (R_P) to make radiating patch. Similarly, the ground layer is designed by elliptical ground (E_P) and rectangular

ground (R_P) to construct the partial ground plane (PGP). Dimensions of E_P and R_P are $\pi \times 8 \times 4$ cm^2 and 8×5 cm^2, respectively while E_G and R_G have dimensions of $\pi \times 8 \times 3.46$ cm^2 and 8×7.34 cm^2, respectively. A 14.39 mm long and $W_s = w_f$ =3.16 mm wide slot is designed on PGP. So, frequency vs. gain and impedance matching are improved.

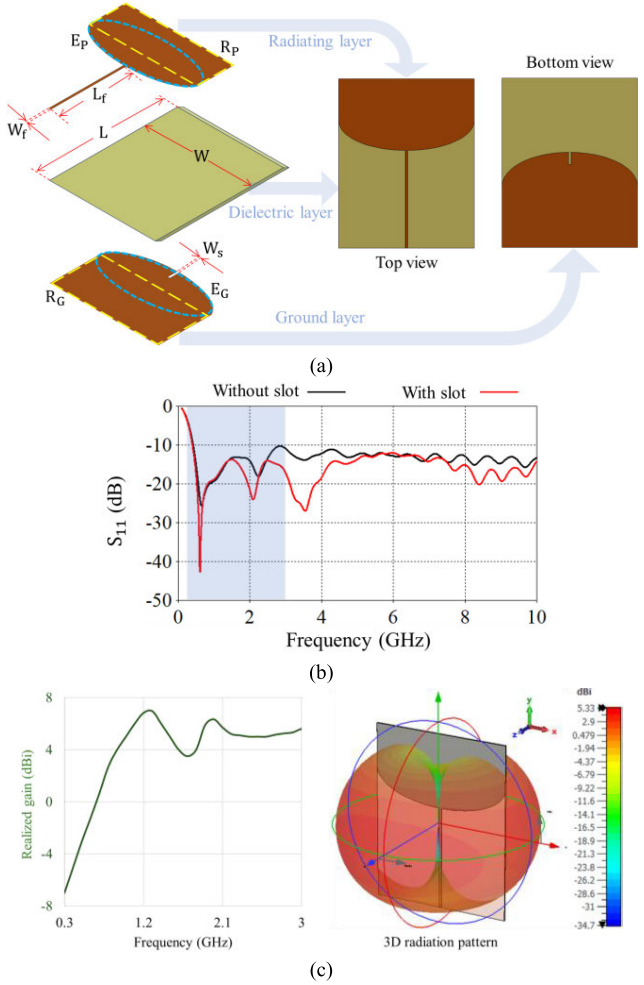

FIGURE 3. MESA simulation: (a) design (b) S_{11} (c) radiation characteristics.

In Fig. 3(b), impact of the slot is observed (in the UHF range of shadowed area). The MESA is further simulated for its realized gain and radiation pattern. In Fig. 3(c), simulated results show that MESA maintains an average realized gain above 2 dBi throughout UHF range within entire bandwidth by maintaining an omnidirectional radiation pattern.

Antenna sensitivity in PD diagnosis can be expressed by UHF antenna's effective height [4]. A complicated Gigahertz Transverse Electromagnetic (GTEM) cell arrangement is needed to determine the height, but it is expensive and unpopular. So, another index of antenna sensitivity is used here to determine the PD detection sensitivity (S_{AS}) as [27],

$$S_{AS} = \left(\frac{G_{Avg.}}{A_P}\right). \tag{8}$$

In this expression, the average realized gain is denoted by $G_{Avg.}$ and antenna-sensor's physical aperture area is denoted by A_P. Another index, as stated in [27], can be utilized to calculate the antenna-sensor's Figure of Merit (FoM_{AS}) as,

$$\text{FoM}_{\text{AS}} = 10 \times \log_{10}\left[\left(\frac{\eta_{\text{Avg.}} \times C_{\text{UHF}}}{100\% \times 100\%}\right) / \left(\frac{4\pi \times A_P}{\lambda_0^2}\right)\right] \tag{9}$$

Here, $\eta_{Avg.}$ is average efficiency and C_{UHF} is UHF bandwidth coverage. FoM_{AS} in (9) expresses the overall performance of a sensor in PD diagnosis. It is noteworthy from (8) and (9) that neither of these sensitivity indexes require any additional complex GTEM cell arrangement. Typical measurement of antenna parameters is sufficient to find out these sensitivity indexes. Hence, (8) and (9) are utilized in this work to find out the sensitivity levels of the UHF antenna.

B. FABRICATION AND MEASUREMENT

The proposed MESA is fabricated as a sensor prototype for PD diagnosis. The prototype was measured in the MRG Lab at the Universiti Teknikal Malaysia Melaka (UTeM). Fig. 4 shows the MESA measurement and results. Bandwidth was measured by the Keysight E5071C ENA VNA, while gain and radiation pattern were measured in a standard non-interference chamber. As in Fig. 4(a), the sensor under test (SUT) was positioned at distance (R) of 4 m from the transmitting (T_X) antenna. Fig. 4(a-b) show that there is a fine agreement between simulated and measured results in terms of bandwidth (BW_{UHF}) in the UHF range, realized gain, and radiation pattern.

In Table 1, MESA performance is compared with other UHF sensors where results are obtained from standard antenna measurements. Commercial antennas typically use amplifiers to compensate for low gain against wide bandwidth. Whereas MESA offers decently high gain yet keeping wide bandwidth performance. Hence, in terms of FoM_{AS} which includes all antenna parameters, MESA demonstrates better performance than conventional UHF antennas in PDD applications.

TABLE 1. MESA performance compared with other UHF sensors.

Ref.	C_{UHF} (%)	BW_{UHF} (GHz)	$G_{Avg.}$ (dBi)	A_P (cm^2)	S_{AS} (dBi/m^2)	FoM_{AS} (dB)
[8]	40.74	0.60–1.70	4.00	$\pi \times 20^2 \times 16$ cm	31.83	−16.67
[9]	43.33	0.31–1.48	2.00	30×30	22.22	–
[10]	38.14	0.35–1.38	3.50	24×20	72.91	−7.18
[11]	98.51	0.34–3.00	3.63	34×14	76.26	–
MESA	97.03	0.38–3.00	3.66	20×16	114.38	−2.71

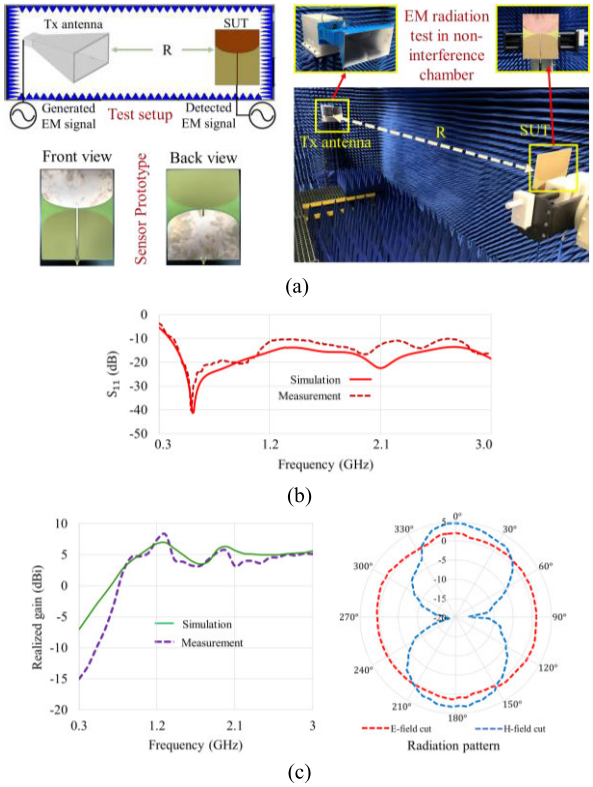

FIGURE 4. MESA measurement: (a) test set up, prototype, and test bench photograph (b) bandwidth performance (c) radiation performance.

V. EXPERIMENTAL SETUP FOR PD PHENOMENA INTERPRETATION

Three different PD defects are used, namely, a void defect (immerged into insulation silicone oil to prevent the test cell from behaving as a surface defect), a surface, and a free wire, as illustrated in Fig. 5. Since this research investigates the EM behaviors in open substation under HVAC and HVDC, these three distinct PD defects are chosen to demonstrate the diverse effects of different types of voltage applied to each particular PD defect. So, the risk level i.e., breakdown of equipment can be predicted at early stages by understanding EM behaviors of these defects in different voltage conditions. Switchgears, cable joints and busbars in practical HV sites encounter these defects mostly e.g., mistaken exposure of a conductor as a free-wire, manufacturing defect as a void bubble inside insulation etc. In Fig. 5(a), the free wire has a diameter of 0.16 cm and length of 31.5 cm (with no sharp end), whereas a polymer disc of 0.2 cm thickness and 5 cm diameter is utilized to make the surface defect. The connection diagram in Fig. 5(b) illustrates the full experimental setup to characterize radiated EM signals from these PD sources. Different HV conditions are delivered to a PD defect by connecting points 1 and 2. Faraday cage is used to protect the test-bench from unwanted signals. In HVDC setup, the 25 nF capacitor was used to smooth the rippled DC voltage after rectifying the supplied AC voltage. In other words, the capacitor is only used as a smoothing capacitor to deliver a flattened HVDC to a testing PD defect. Note, this capacitor does not affect the electromagnetic radiation of a PD defect because it only prevents the HVDC supply from unwanted fluctuations before initiating a PD event [28], [29].

Test-cells are calibrated by coupling capacitor-based IEC 60270 standard. For each calibration, corresponding voltage values are recorded both by the coupling capacitor and the UHF antenna so that these values are utilized to initially estimate antenna's ability of PD detection. In the PD measurement chain, we have made a stepwise variation of the distance (D) between PD defect and UHF sensor to obtain corresponding characterization results. As described in section III-A, the EM radiation pattern of PD defects is omnidirectional. So, the D has been varied at different axial positions but fixed in one radial direction. It is important to note that any PD event is detected from these distances regardless of its time and frequency contents of the EM radiation because PD in the UHF range does not occur at a single frequency. Rather, PD keeps occurring at different frequencies within the UHF range, depending on the applied voltage, defect's formation, and surrounding environmental conditions [4]. Since our designed UHF sensor operates with a bandwidth that covers more than 97% of the UHF range, almost every PD event is captured by placing the sensor at various distances from these defects under different voltages.

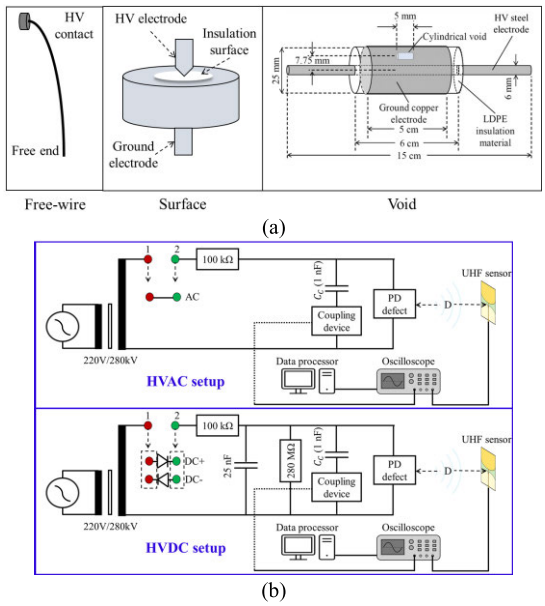

FIGURE 5. Schematic: (a) PD defects (b) PD test setup in HVAC and HVDC.

VI. MEASURED PD PHENOMENA RESULTS AND EM INTERPRETATIONS

A. INITIAL CONDITIONS IN PD DEFECTS

Initially, when a static charge is calibrated to a PD defect, UHF sensor can detect a corresponding signal at a consistent voltage. This detected voltage is a resultant of electric field only because the calibrated charge, being static, does not generate magnetic field. So, when calibrated charges are applied, the UHF sensor detects electric field voltages in the Fresnel

region. Electric and magnetic fields can exist separately and are detectable in the Fresnel region [13]. Now, for the calibrated charges, our UHF sensor is placed at 1 m distance from PD defects to wirelessly detect the corresponding peak-to-peak voltage (V_{PP}) in Fresnel region while collecting V_{PP} by the coupling capacitor (C_C) as illustrated previously in Fig. 5(b). Next, with the UHF sensor, V_{PP} is detected from HV sparks that generates EM radiation through accelerated charges between two electrodes in a gap. Distance varies by 1–10 m so that far-field radiation is examined to find the range of D variation. As observed in Fig. 6(a), the V_{PP} of electric field detected by the UHF antenna-sensor is found to be highest for the surface defect. In fact, for the surface defect, V_{PP} by the UHF antenna-sensor is more than V_{PP} by the coupling capacitor in case of all calibrated charges.

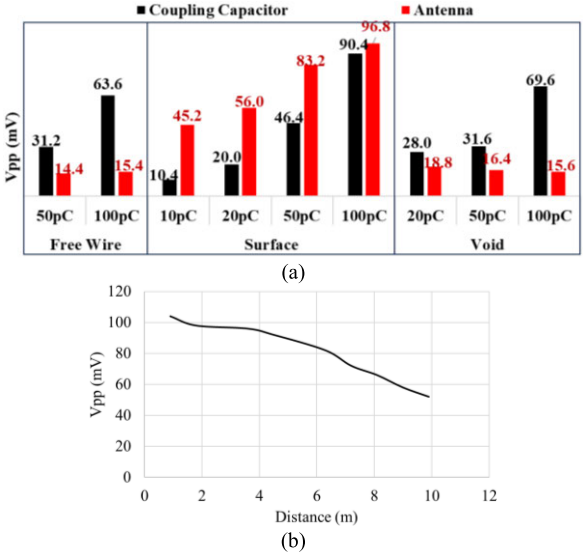

FIGURE 6. Detected voltages from (a) calibrated charges, (b) HV sparks.

Surface defects typically have a conductor-dielectric-conductor structure, creating capacitive effects. In our test object, the surface defect features a sharp-tipped HV conductor, reducing capacitive effects and allowing the electric field voltage to increase with added calibrated charges, resulting in a high V_{PP}. For the void defect, a similar increase in V_{PP} is observed by the coupling capacitor, but the V_{PP} detected by the UHF antenna-sensor remains almost unchanged despite increased calibrated charges. This is because the coupling capacitor detects V_{PP} through direct electrical contact with the defect, whereas the UHF antenna-sensor detects it via the wirelessly distributed electric field. Since this particular void is surrounded by insulating material and also submersed inside insulation oil, V_{PP} detected from the electric field is immediately attenuated and weakened. Also, adding more static charges to the void defect increases the capacitance. Consequently, V_{PP} does not tend to increase while increasing calibrated charges to the void defect. In the case of adding calibrated charges to the free wire defect, the electric field becomes weak due to the absence of a ground connection and the low dielectric permittivity of air. Thus, the electric field is not intensified which results in low V_{PP} even for increasing charges. However, V_{PP} from the coupling capacitor increases for the direct electrical connection. It is important to remember that V_{PP} detected by antenna is due to the prominent electric field formed by the calibrated static charges. So, these PD defects with static charges do not fully demonstrate electromagnetic behavior [23], [24]. In Fig. 6(b), V_{PP} is plotted with the UHF sensor distances at 1–10 m from an HV spark generator. The graph shows a declining trend of V_{PP} versus distance (D). So, considering V_{PP} values declining with respect to increasing the distance at the EM far field radiation, variation of D has been considered within 1–4 m for the EM characterization to keep the sensitivity high. Gain enhancement techniques can be used to improve sensitivity of detecting PD even from longer distances.

PD inception voltage (PDIV) and corresponding V_{PP} detected at different distances (D) from each defect are presented in Fig. 7. For free wire, PDIV is 21 kV in HVAC, while it is 3 kV in HVDC+ and HVDC–. This is because HVAC alters the polarity, delaying charge acceleration and requiring higher voltage to initiate PD in the free wire. In HVDC+ and HVDC–, charge acceleration occurs faster without polarity alteration, and there is no ground connection in a free wire defect. This affects the detected V_{PP}, as shown in Fig. 7(b), where V_{PP} is higher under HVDC+ and HVDC– conditions. In the free wire, V_{PP} decreases with increasing D. For the surface defect, the capacitive effect is more pronounced due to the metal-dielectric-metal configuration, lowering PDIV in HVAC but raising it in HVDC+ and HVDC–, as shown in Fig. 7(a). Thus, despite increasing D when HVAC is applied, V_{PP} tends to increase up to a 4-meter distance at PDIV. This indicates that far-field EM radiation at PDIV in HVAC is intensified by the combination of point charge acceleration and dipole effects, particularly for surface defects. In void defects, the overall variation with respect to D is similar to surface defects at PDIV.

Although surface and void defects exhibit similar capacitive effects, their EM radiations differ because the void defect is submerged in HV insulation oil with different dielectric permittivity. So, it is important to characterize EM behavior of these PD defects under different applied voltages.

B. FREE WIRE DEFECT CHARACTERISTICS

As indicated before, free wire defects are mostly point charge-based, with EM radiation depending on charge acceleration. EM radiation also heavily depends on the dimensions of a PD defect. Thus, for a specific PD defect, variations in distance (D) and partial discharge applied voltage (PDAV) characterize its EM radiation. Fig. 8 characterizes free wire defects in terms of V_{PP} collected by the UHF antenna-sensor. As shown in Fig. 8(a), V_{PP} is always detected as lower than 40 mV from any distance, even when the applied HVAC is increased close to the breakdown. This validates the fact that the continuous alteration of polarity in HVAC does not

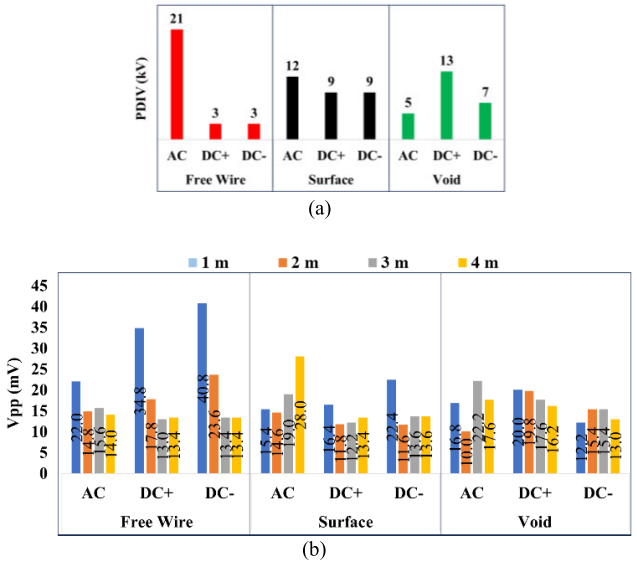

FIGURE 7. Initial conditions; (a) different PDIVs (b) V_{PP} for PDIV at 1–4 m.

allow point charges to radiate with more EM power through uninterrupted acceleration, as inferred in (4). Therefore, throughout the D variation, V_{PP} does not change much, even though PDAV varies significantly over 21–61 kV. In contrast, during HVDC+ and HVDC–, as shown in Fig. 8(b) and Fig. 8(c), V_{PP} values are noticeably high and vary with D. In HVDC+, V_{PP} increases with increasing applied voltages within the range of 3–18 kV. A similar observation is found in HVDC– within the 3–14 kV applied voltage range. Additionally, PDIV is found to be as low as 3 kV, and breakdown occurs quickly with increased applied voltage. Note, point charge acceleration occurs more in HVDC+ and HVDC– due to the absence of polarity alteration, resulting in more EM power radiation as previously expressed in (4). According to (4), it is obvious that radiated EM power proportionally increases with the square of a point charge. A point charge accelerates with higher magnitude when HVDC is applied because the absence of polarity alteration keeps allowing the charge to increase its value. In turn, an accelerated point charge with a higher magnitude radiates with stronger EM power in HVDC compared to HVAC. In HVDC, V_{PP} tends to increase rapidly over time as charge acceleration regeneratively increases without finding a direct ground path in a free wire defect. This leads to earlier and faster breakdown, making free wire defects the riskiest for HVDC substations.

C. SURFACE DEFECT CHARACTERISTICS

In surface defects, there are dipole, point charge acceleration, and a combination of both. Besides air, another dielectric medium exists in surface defects, touched by both the HV conductor and the ground conductor. This structure intensifies EM radiation due to the capacitive effect of the conductor-dielectric-conductor configuration, in addition to the combined effects of dipole and point charge acceleration.

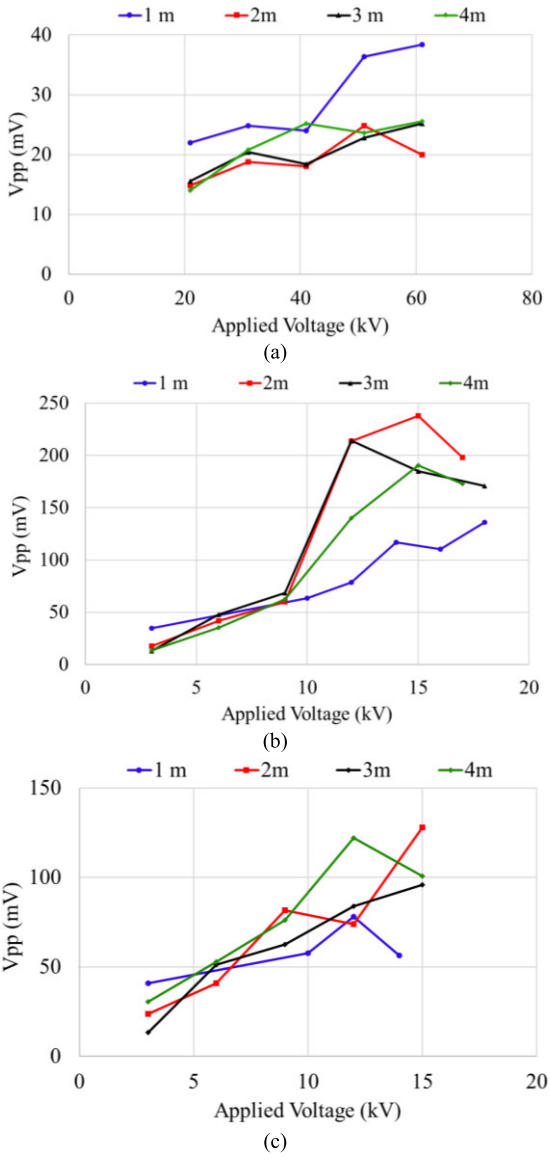

FIGURE 8. Free wire characteristics: (a) HVAC (b) HVDC+ (c) HVDC–.

Different HV conditions alter these effects in a surface defect, leading to variations in V_{PP} detected at different distances. Fig. 9 illustrates the characteristics of surface defects under HVAC, HVDC+, and HVDC– conditions.

When HVAC is applied to a surface defect, V_{PP} is highest when detected from the closest distance in the far-field region, indicating very intense EM radiation nearby. Fig. 9(a) shows the detected V_{PP} for different applied HVAC voltages from 1–4 meters. Applied HVAC alters polarities for point charge accelerations, which restricts V_{PP} from increasing quickly, whereas the same alteration increases V_{PP} caused by dipole discharges in the dielectric medium. Dipole discharges are short-term, as indicated by (5), resulting in a high total V_{PP} amplitude. So, as inferred by (6), overall EM radiation is intensified at HVAC, especially at close distances (1–2 meters) within the far-field. In Fig. 9(b) and Fig. 9(c) at HVDC+ and HVDC–, the absence of polarity alteration

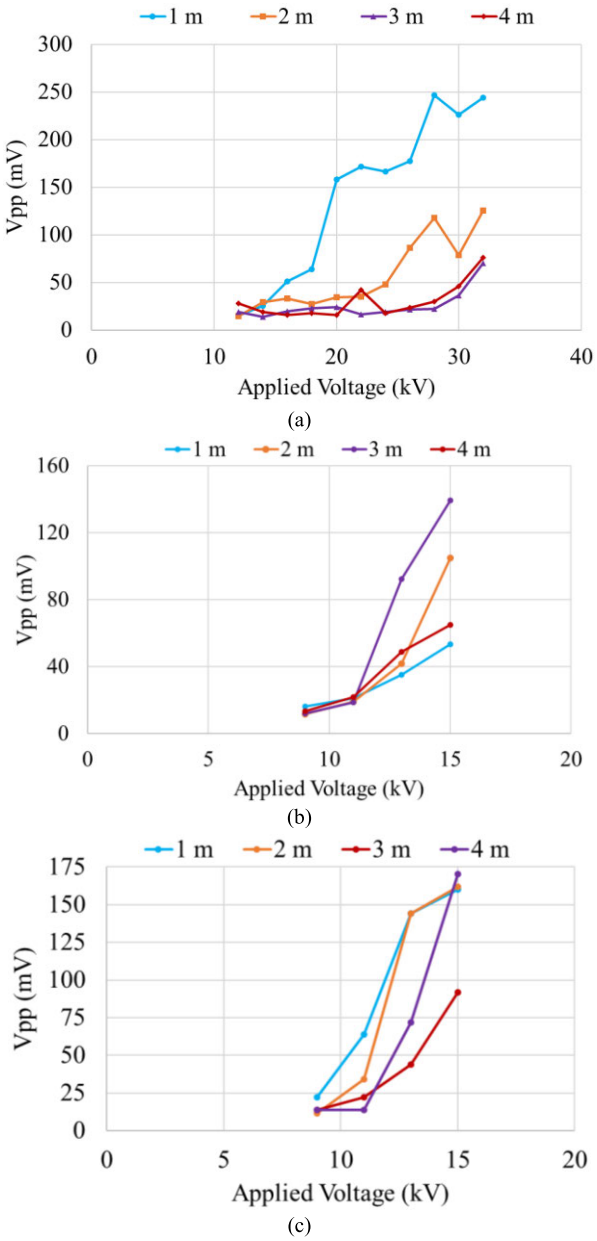

FIGURE 9. Surface characteristics: (a) HVAC (b) HVDC+ (c) HVDC−.

reduces dipole discharges in the dielectric medium, but regenerates point charge acceleration in conductors exposed to air. Therefore, the overall V_{PP} remains high but lower than in the HVAC condition. Also, PD occurs less frequently within a short range of applied voltages (9–15 kV).

D. VOID DEFECT CHARACTERISTICS

Void defects have some similar EM features to surface defects. Fig. 10 shows the characteristics of void defects under different HV conditions. In HVAC, void defects behave similarly to surface defects. As seen in Fig. 10(a), V_{PP} is maximum at close distances (1–2 meters) within the far-field region. Like surface defects in HVAC, polarity alteration improves V_{PP} by enhancing void dipole discharges. In this case, the defect is immersed in silicone oil, a different dielectric medium than air. This configuration causes the entire defect structure to radiate more EM power with higher voltage magnitude because the T_H becomes even shorter with polarity alteration in HVAC.

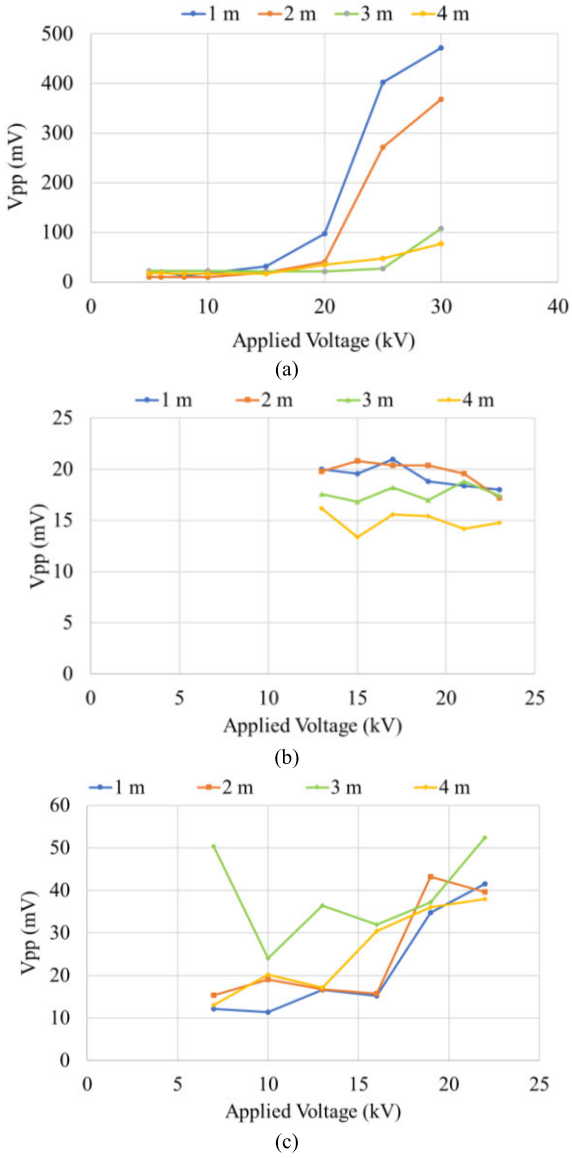

FIGURE 10. Void characteristics: (a) HVAC (b) HVDC+ (c) HVDC−.

Because of polarity reversal in HVAC, both surface and void defects radiate more EM power since T_H is shorter. However, the radiated EM power gradually starts weakening when it propagates beyond some distances 1-2 meters in this case) in the far-field region. It is because the propagation encounters a damping effect due to direct contact with stronger dielectric insulating mediums than air. Whereas in HVDC conditions, V_{PP} does not reach as high as in HVAC because T_H is longer in this case due to the absence of polarity reversal. In Fig. 10(b) and Fig. 10(c), when silicone oil submerges the void defect at HVDC, it prevents

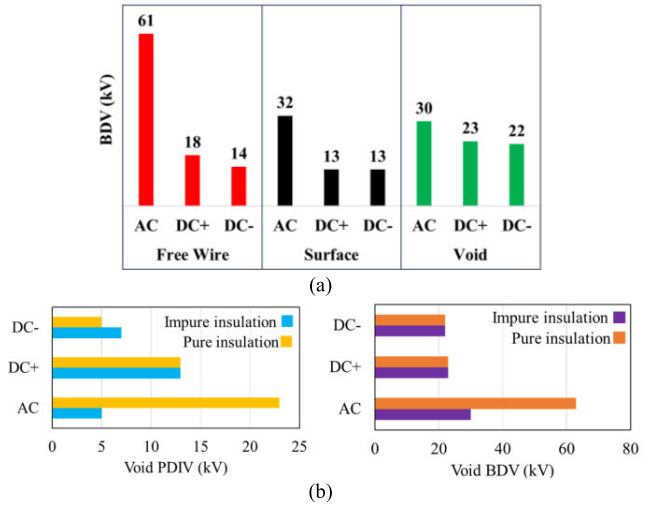

FIGURE 11. Final condition; (a) different BDV (b) effects of insulation purity.

the point charge acceleration from regenerating around the void. Hence, EM power rapidly dissipates inside the oil and further weakens EM radiation in the far field distances. This is how silicone oil submersion affects differently in HVAC and HVDC conditions. Despite having radiation similarities of surface and void defects in HVAC, these defects radiate differently in HVDC. For instance, unlike surface defects in HVDC+, void defects do not start generating loud sounds before breakdown happens.

E. FINAL CONDITIONS IN PD DEFECTS

PD defects experience complete insulation breakdown when the applied voltage reaches the level that causes a full discharge through the insulation, known as breakdown voltage (BDV). Since BDV varies from one PD defect to another depending on their dimensions and types, we have determined the BDV of a PD defect by gradually increasing applied voltages to the defect [28], [29]. Until a breakdown occurs to a PD defect, an impulse signal is observed in the oscilloscope's monitor. While increasing the applied voltage, suddenly a flashover response is observed in the monitor when the breakdown occurs. So, BDV of a particular defect has been determined by recording the final voltage when a flashover response is observed instead of a single impulse in oscilloscope's monitor. Meanwhile, EM characteristics of PD defects are influenced by dipole and point charge acceleration, which also affect BDV. Since point charge acceleration is highest in free wire defects, BDV occurs faster in any HV conditions due to the ungrounded open end of a free wire defect, which regenerates the charge acceleration. Consequently, PD occurs frequently, and loud sounds are generated during the final stage of a free wire defect. Fig. 11(a) presents BDV in different defects and HV conditions. As previously inferred, BDV is the highest (61 kV) for free wire in HVAC. This is also true for surface and void defects under HVAC, despite not being solely composed of point charge acceleration like free wire defects. In HVDC+ and HVDC–, the corresponding BDVs of these defects are much lower than in HVAC. Unlike free wire and surface defects, breakdown in void defects is neither visible nor audible unless the PD magnitude is high. In open substations, insulation purity plays a vital role in BDV. Fig. 11(b) shows the effects of insulation purity on PDIV and BDV during void defects. The void defect was immersed in insulating oil slightly contaminated with environmental impurities to avoid unwanted discharges surrounding the test object. This ensured that PD occurred from within the void, not elsewhere. The experiment was repeated with pure insulation to compare the effects of insulation purity. As shown in Fig. 11(b), insulation purity significantly reduces PDIV and BDV in HVAC. However, in HVDC+ and HVDC–, PDIV and BDV remain almost unchanged.

Table 2 summarizes the EM characteristics interpretation of PD defects and provides some take-home remarks.

TABLE 2. EM characteristics of PD defects: summary and remarks.

HV	Free wire defect	Surface defect	Void defect
AC	EMR* by PCA*; high BDV	Strong EMR in close distance of far-field by PCA and dipole	Strong EMR in close distance of far-field by PCA and dipole
DC+	EMR from regenerated PCA; fast breakdown	EMR by PCA and dipole; PD amplitude reduces over time; loud noise	Weak EMR as EM power dissipates inside insulation
DC–	EMR from regenerated PCA; fast breakdown	EMR by PCA and dipole; less PD occurs; low BDV	Weak EMR as EM power dissipates inside insulation

*EMR = Electromagnetic radiation; *PCA = point charge acceleration.

VII. CONCLUSION

In this work, three common PD defects, i.e., free wire, surface, and void defects with particular dimensions, are experimentally interpreted in terms of electromagnetic (EM) radiation characteristics from dipole and point charge acceleration. A new passive UHF sensor is developed by a modified elliptic-shaped antenna (MESA) on a low-cost FR-4 substrate. The antenna-sensor has a performance Figure of Merit of –2.71 dB which surpasses similar other antenna-sensors for PD application. Experiments were conducted under different HV conditions on the laboratory scale. It is found that EM radiation is different with the variation of distance and applied voltage even for the same defect. So, the characterization is performed by varying the distance between the UHF sensor and each specific defect in different HV conditions. Hence, the EM characteristics interpretation in this work is rigorous, in-depth, and insightful from theoretical and experimental perspectives at the same time. This work characterizes practical sensing tests in terms of theoretical models. Experimental results have been interpreted based on

the theory of electromagnetic radiation from different partial discharge defects. Novelty and key contributions of this work can be summarized as:

- Experimental investigation of EM characteristics for different PD defects at variable distances in HVAC and HVDC has been performed for the first time.
- A new UHF sensor has been developed which offers better sensitivity (114.38 dBi/m^2), figure of merit (-2.71 dB), and UHF coverage ability (97.07%) than other sensors in the same scope.
- Impacts of distance on PD sensing from EM far field radiation have been revealed for three defects under three different voltage conditions.

The next step of this work is to perform the localization of partial discharge defects and improve the localization accuracy by machine learning techniques. In the localization, by using the same specification as the proposed MESA, we are going to detect EM signals by four UHF sensors placed at different distances from a PD defect. Therefore, this paper is especially insightful for improving the PD localization accuracy because its results indicate the impacts of different sensing distances during PD detection.

REFERENCES

[1] E. N. Tziris, P. I. Lazaridis, Z. D. Zaharis, J. P. Cosmas, K. K. Mistry, and I. A. Glover, "Optimized planar elliptical dipole antenna for UWB EMC applications," *IEEE Trans. Electromagn. Compat.*, vol. 61, no. 4, pp. 1377–1384, Aug. 2019.

[2] M. Au, B. L. Agba, and F. Gagnon, "A model of electromagnetic interferences induced by corona discharges for wireless channels in substation environments," *IEEE Trans. Electromagn. Compat.*, vol. 57, no. 3, pp. 522–531, Jun. 2015.

[3] S. M. K. Azam, M. Othman, H. A. Illias, T. A. Latef, D. Fahmi, W. J. K. Raymond, W. N. L. Wan Mahadi, A. K. M. Z. Hossain, M. Z. A. Abd. Aziz, and A. Ababneh, "Unknown PD distinction in HVAC/HVDC by antenna-sensor with pulse sequence analysis," *Alexandria Eng. J.*, vol. 91, pp. 457–471, Mar. 2024.

[4] S. M. K. Azam, M. Othman, H. A. Illias, T. A. Latef, M. T. Islam, and M. F. Ain, "Ultra-high frequency printable antennas for partial discharge diagnostics in high voltage equipment," *Alexandria Eng. J.*, vol. 64, pp. 709–729, Feb. 2023.

[5] M. Koziol, M. Kunicki, I. Urbaniec, L. Nagi, O. Kabot, and L. Klein, "Analysis of radio frequency and ultraviolet signals emitted by surface partial discharges," in *Proc. 23rd Int. Sci. Conf. Electric Power Eng. (EPE)*, May 2023, pp. 1–4.

[6] S. Tenbohlen, D. Denissov, S. Hoek, and S. M. Markalous, "Partial discharge measurement in the ultra high frequency (UHF) range," *IEEE Trans. Dielectr. Electr. Insul.*, vol. 15, no. 6, pp. 1544–1552, Dec. 2008.

[7] J. Q. Chan, W. J. K. Raymond, H. A. Illias, and M. Othman, "Partial discharge localization techniques: A review of recent progress," *Energies*, vol. 16, no. 6, p. 2863, Mar. 2023.

[8] S. Park and K.-Y. Jung, "Design of a circularly-polarized UHF antenna for partial discharge detection," *IEEE Access*, vol. 8, pp. 81644–81650, 2020.

[9] G. V. R. Xavier, E. G. da Costa, A. J. R. Serres, L. A. M. M. Nobrega, A. C. Oliveira, and H. F. S. Sousa, "Design and application of a circular printed monopole antenna in partial discharge detection," *IEEE Sensors J.*, vol. 19, no. 10, pp. 3718–3725, May 2019.

[10] Y. Zhang, P. Lazaridis, R. Abd-Alhameed, and I. Glover, "A compact wideband printed antenna for free-space radiometricdetection of partial discharge," *TURKISH J. Electr. Eng. Comput. Sci.*, vol. 25, no. 2, pp. 1291–1299, 2017.

[11] J. D. N. Cruz, A. J. R. Serres, A. C. de Oliveira, G. V. R. Xavier, C. C. R. de Albuquerque, E. G. da Costa, and R. C. S. Freire, "Bio-inspired printed monopole antenna applied to partial discharge detection," *Sensors*, vol. 19, no. 3, p. 628, Feb. 2019.

[12] X. Kong, C. Zhang, B. Du, C. Hou, Y. Chen, and J. Jiang, "An improved UHF antenna for partial discharge detection based on coplanar waveguide feeding," in *Proc. IEEE 4th Int. Conf. Electr. Mater. Power Equip. (ICEMPE)*, vol. 50, May 2023, pp. 1–4.

[13] S. M. K. Azam, M. Othman, H. A. Illias, T. A. Latef, W. N. L. W. Mahadi, D. Fahmi, A. K. M. Z. Hossain, and M. F. Ain, "Planar sensor for noise cancellation during partial discharge detection in open substation," *IEEE Sensors J.*, vol. 23, no. 14, pp. 15552–15562, Jul. 2023.

[14] C. Li, T. Shahsavarian, M. A. Baferani, K. Davis, Y. Cao, and D. Zhang, "Understanding DC partial discharge: Recent progress, challenges, and outlooks," *CSEE J. Power Energy Syst.*, vol. 8, no. 3, pp. 894–909, May 2022.

[15] Y. Zhao, S. Zheng, X. Yan, and J. Kong, "Study on the electromagnetic characteristics of two different types of partial discharge at the initial stage," in *Proc. IEEE 6th Int. Electr. Energy Conf. (CIEEC)*, May 2023, pp. 944–948.

[16] R. Piccin, A. R. Mor, P. Morshuis, A. Girodet, and J. Smit, "Partial discharge analysis of gas insulated systems at high voltage AC and DC," *IEEE Trans. Dielectr. Electr. Insul.*, vol. 22, no. 1, pp. 218–228, Feb. 2015.

[17] Y. R. Yadam, R. Sarathi, and K. Arunachalam, "Numerical and experimental investigations on influence of internal defect parameters on partial discharge induced UHF signals in gas insulated switchgear," *IEEE Access*, vol. 10, pp. 110785–110795, 2022.

[18] P. Wenger, M. Beltle, S. Tenbohlen, U. Riechert, and G. Behrmann, "Combined characterization of free-moving particles in HVDC-GIS using UHF PD, high-speed imaging, and pulse-sequence analysis," *IEEE Trans. Power Del.*, vol. 34, no. 4, pp. 1540–1548, Aug. 2019.

[19] D. Zhou, X. Yang, Z. Ma, L. Cai, B. Tai, B. Tai, Y. Jin, C. Lin, S. Jiang, X. Shu, H. Liu, and G. Ma, "Simulation study on UHF signal propagation characteristics of partial discharge in the power transformer outlet device," in *Proc. IEEE 4th Int. Conf. Electr. Mater. Power Equip. (ICEMPE)*, May 2023, pp. 1–4.

[20] R. Sarathi, A. J. Reid, and M. D. Judd, "Partial discharge study in transformer oil due to particle movement under DC voltage using the UHF technique," *Electr. Power Syst. Res.*, vol. 78, no. 11, pp. 1819–1825, Nov. 2008.

[21] S. Suwan, T. Tiengthong, P. Southisombath, and S. Promwong, "Characterization of electromagnetic wave in transformer for partial discharge detection," in *Proc. 9th Int. Conf. Eng., Appl. Sci., Technol. (ICEAST)*, Jun. 2023, pp. 209–212.

[22] R. Albarracín, J. Ardila-Rey, and A. Mas'ud, "On the use of monopole antennas for determining the effect of the enclosure of a power transformer tank in partial discharges electromagnetic propagation," *Sensors*, vol. 16, no. 2, p. 148, Jan. 2016.

[23] A. Bojovschi, W. Rowe, and A. K. L. Wong, "Electromagnetic field intensity generated by partial discharge in high voltage insulating materials," *Prog. Electromagn. Res.*, vol. 104, pp. 167–182, 2010.

[24] A. Darwish, S. S. Refaat, H. A. Toliyat, and H. Abu-Rub, "On the electromagnetic wave behavior due to partial discharge in gas insulated switchgears: State-of-Art review," *IEEE Access*, vol. 7, pp. 75822–75836, 2019.

[25] Y. Shibuya, S. Matsumoto, T. Konno, and K. Umezu, "Electromagnetic waves from partial discharges in windings and their detection by patch antenna," *IEEE Trans. Dielectr. Electr. Insul.*, vol. 18, no. 6, pp. 2013–2023, Dec. 2011.

[26] Y. Shibuya, S. Matsumoto, M. Tanaka, H. Muto, and Y. Kaneda, "Electromagnetic waves from partial discharges and their detection using patch antenna," *IEEE Trans. Dielectr. Electr. Insul.*, vol. 17, no. 3, pp. 862–871, Jun. 2010.

[27] M. S. Islam, S. M. K. Azam, A. K. M. Z. Hossain, M. I. Ibrahimy, and S. M. A. Motakabber, "A low-profile flexible planar monopole antenna for biomedical applications," *Eng. Sci. Technol., Int. J.*, vol. 35, Nov. 2022, Art. no. 101112.

[28] D. Fahmi, H. A. Illias, H. Mokhlis, and I. M. Y. Negara, "Negative DC corona patterns for different wire particle geometries in air insulation," *Alexandria Eng. J.*, vol. 73, pp. 635–649, Jul. 2023.

[29] D. Fahmi, H. A. Illias, H. Mokhlis, and I. M. Y. Negara, "Particle-triggered corona discharge characteristics in air insulation under DC voltage," *IEEE Trans. Dielectr. Electr. Insul.*, vol. 30, no. 2, pp. 658–666, Apr. 2023.

S. M. KAYSER AZAM was born in Pabna, Bangladesh. He received the B.Sc. degree in electrical and electronic engineering from Khulna University of Engineering and Technology (KUET), Bangladesh, in 2013, the M.Sc. degree in electronics engineering from International Islamic University Malaysia (IIUM), Kuala Lumpur, Malaysia, in 2019, and the Doctor of Philosophy from the Department of Electrical Engineering, Universiti Malaya (UM), Kuala Lumpur, in 2024.

He was a Power Engineer with Huawei Technologies Bangladesh Ltd., from 2014 to 2016. He has authored or co-authored many papers in reputable journals and conferences. His research interests include applied electromagnetics, antenna, microwave components, wireless technologies, and electronics. He has served as a Reviewer for IEEE TRANSACTIONS ON CIRCUITS AND SYSTEMS II: EXPRESS BRIEFS and IEEE ACCESS.

JUN QIANG CHAN was born in Melaka, Malaysia. He received the B.Eng. degree (Hons.) in electrical and electronic engineering from Tunku Abdul Rahman University College, Malaysia, in 2020. He is currently pursuing the M.Eng.Sc. degree in electrical engineering with Universiti Malaya, Kuala Lumpur, Malaysia.

He was a Graduate Trainee and a Hardware Engineer of Intel Microelectronics (M) Sdn. Bhd., from 2020 to 2021. His research interests include partial discharge measurement, localization, and artificial intelligence techniques.

MOHAMADARIFF OTHMAN received the B.Eng. degree (Hons.) in electronic engineering from Multimedia University, Malaysia, in 2006, and the M.Sc. degree in RF and microwave and the Ph.D. degree in antenna and propagation from Universiti Sains Malaysia (USM), Malaysia, in 2008 and 2015, respectively.

He has been with the Department of Electrical Engineering, Universiti Malaya, Malaysia, as a Senior Lecturer, since 2016. Prior to that, he was a Lecturer with UCSI University, Malaysia for almost 1.5 years. His research interests include 5G antennas, dielectric characterization, dielectric resonator antenna design, and antenna design optimization. He is a member of the Board of Engineers Malaysia.

WONG JEE KEEN RAYMOND (Senior Member, IEEE) received the Bachelor of Electrical and Electronics Engineering (Hons.) and Master of Electrical Engineering degrees from Universiti Tenaga Nasional, in 2010 and 2013, respectively, and the Ph.D. degree from Universiti Malaya, in 2016.

He was a Product Engineer with Motorola Solutions, from 2010 to 2011, a Senior Lecturer, from 2016 to 2018, and a Program Leader with Tunku Abdul Rahman University College, 2019-2021. Since 2021, he has been a Senior Lecturer with Universiti Malaya. He is currently a Chartered Engineer (C.Eng. U.K.) and a Professional Engineer (P.Eng. BEM). His research interests include insulation condition monitoring, partial discharge phenomenon, machine learning, and deep learning for fault localization and classification. He is a member of the Institution of Engineering and Technology (IET) and the Institution of Engineers Malaysia (IEM), and a Professional Technologist of Malaysia Board of Technologists (MBOT). He has been an Honorary Secretary for the IEEE Dielectrics and Electrical Insulation Society (DEIS), Malaysia, since 2020.

HAZLEE AZIL ILLIAS (Senior Member, IEEE) received the bachelor's degree in electrical engineering from Universiti Malaya, Kuala Lumpur, Malaysia, in 2006, and the Ph.D. degree in electrical engineering from the University of Southampton, Southampton, U.K., in 2011.

Since 2011, he has been an Academic Staff with the Department of Electrical Engineering, Universiti Malaya, and the Head of the UM High Voltage Research Group (UMHVRG). He is currently registered as a Chartered Engineer (C.Eng. U.K.) and Professional Engineer (P.Eng. Mal). His research interests include modeling and measurement of partial discharge in solid dielectric insulation, lightning overvoltage, transmission line modeling, optimization methods, and artificial intelligence. He is a member of the Institution of Engineering and Technology and a Corporate Member of the Institution of Engineers Malaysia.

TARIK ABDUL LATEF received the B.Sc. degree in electrical and electronic engineering from the University of Oita, Japan, in 1997, the M.Sc. degree in electrical engineering from the University of Leeds, in 2005, and the Ph.D. degree from The University of Sheffield, U.K., in 2011.

He is currently a Senior Lecturer with the Department of Electrical Engineering, Faculty of Engineering, University of Malaya, Malaysia. His research interests include circularly polarized antennas, conformal antennas, frequency independent antennas, array design, dielectric resonator antennas, superconducting metamaterial antennas, and RCS reduction.

A. K. M. ZAKIR HOSSAIN (Member, IEEE) received the B.Sc. degree in electrical and electronic engineering from Rajshahi University of Engineering and Technology (RUET), Bangladesh, in 2007, the Master of Science (M.Sc.) degree in electronics/telecommunications from the University of Gavle, Gavel, Sweden, in 2013, and the Doctor of Philosophy degree in engineering from International Islamic University Malaysia (IIUM), in 2017.

He was a Postdoctoral Research Fellow with International Islamic University Malaysia (IIUM), from 2018 to 2019. He is currently a Senior Lecturer with the Centre for Telecommunication Research and Innovation, Fakulti Teknologi Kejuruteraan dan Elektrik dan Elektronik, Universiti Teknikal Malaysia Melaka (UTeM), Melaka, Malaysia. His research interests include microwave passive devices, chipless RFIDs, microwave passive sensors, MIMO antennas, and 5G mobile communications. He worked on several projects with Ericsson Gavle, Future PositionX, and Chalmars MC2. He has authored more than 30 peer reviewed journal articles and conference papers. He is a Certified Engineering Technologist in the Board of Engineers Malaysia (BEM), a member of the International Association of Engineers (IAENG), and a Graduate Technologist in Malaysian Board of Technologists (MBOT). He is a Reviewer in IEEE ACCESS.

HAMASKUTTY VETTIKALLADI received the Ph.D. degree from Cochin University of Science and Technology, and the Habilitation A Diriger des Recherches degree from the University of Rennes 1, France, in 2018.

He started his career as a Postdoctoral Researcher with the Bell Engineering Department, University of Arkansas, USA, in 2008, just after finishing his Ph.D. degree. From 2008 to 2012, he was a Postdoctoral Fellow with the Institute of Electronics and Telecommunication of Rennes, University of Rennes 1. From 2012 to 2022, he was an Assistant and Associate Professor with King Saud University. Since 2022, he has been a Full Professor with the Department of Electrical Engineering, King Saud University. He is the author of more than 100 scientific publications in international journals and conferences and three book chapters. His main research interests include microwave, millimeter, and THz antenna design for various applications, including high-speed WIFI, automotive radar, imaging, point to point communications, and 5G/6G. He has served as a visiting faculty in several institutes, as an editor, and a referee in scientific journals and conferences.

ALI M. ALMUHLAFI (Senior Member, IEEE) was born in Bisha, Saudi Arabia. He received the B.S. degree in electrical engineering from King Saud University, Riyadh, Saudi Arabia, in 2008, and the M.A.Sc. and Ph.D. degrees from the University of Waterloo, Waterloo, ON, Canada, in 2012 and 2018, respectively.

In 2019, he joined the Department of Electrical Engineering, King Saud University as an Assistant Professor. He is currently an Associate Professor with the Department of Electrical Engineering, King Saud University. He has authored or co-authored more than 31 journal and conference papers on topics related to nondestructive testing, near-field microwave sensors, and microwave imaging. He was awarded the Best Undergraduate Project Award at King Saud University, in 2008. He has also served as a reviewer for several journals.

MOHAMED HIMDI received the Ph.D. degree in signal processing and telecommunications from the University of Rennes 1, France, in 1990.

Since 2003, he has been a Professor with the University of Rennes 1, and the Head of the High Frequency and Antenna Department, IETR, in 2013. He has authored or co-authored 133 journal articles and more than 280 papers in conference proceedings. He has also co-authored nine book chapters. He holds 40 patents. His research activities concern passive and active millimeter-wave antennas. His research interests include the development of new architectures of antenna arrays, and new three-dimensional (3-D) antenna technologies. He was a Laureate of the 2d National Competition for the Creation of Enterprises in Innovative Technologies, Ministry of Industry and Education, in 2000. He received the JEC-AWARD in Paris on Pure Composite Material Antenna Embedded into a Motorhome Roof for the Digital Terrestrial Television Reception, in March 2015.

ABD KARIM ABD RAHMAN is currently a Principal of protection and control with the IRSO East Coast in the Project Delivery and Technology Division, Petroliam Nasional Berhad (Petronas), Kemaman, Terengganu, Malaysia.